Journal of Solid State Chemistry **148,** 479–486 (1999)
Article ID jssc.1999.8483, available online at http://www.idealibrary.com on IDEAL®

Structural, Electronic, and Magnetic Characterization of the Perovskite $LaNi_{1-x}Ti_xO_3$ ($0 \leq x \leq \frac{1}{2}$)

E. Rodríguez, I. Álvarez, M. L. López, M. L. Veiga, and C. Pico

Departamento de Química Inorgánica I, Facultad de Ciencias Químicas, Universidad Complutense, 28040 Madrid, Spain
E-mail: marisal@eucmax.sim.ucm.es

Received March 1, 1999; in revised form July 26, 1999; accepted August 11, 1999

DEDICATED TO PROFESSOR M. GAITÁN ON THE OCCASION OF HIS 70TH BIRTHDAY

Structural, electronic, and magnetic behavior of the $LaNi_{1-x}Ti_xO_3$ ($0 \leq x \leq \frac{1}{2}$) perovskite-like system is reported. These phases can be regarded as derived from $LaNiO_3$ by partial substitution of Ni^{3+} by Ti^{4+} cations that produces a partial reduction of Ni^{3+} to Ni^{2+}. X-ray powder diffraction data were analyzed by the Rietveld method, and rhombohedral (S.G. $R\bar{3}c$) or orthorhombic (S.G. *Pbnm*) symmetry were found depending on the degree of substitution, x. Conductivity and Seebeck measurements show the presence of metal to insulator (M–I) transitions in these oxides and the different nature of the carriers. Magnetic susceptibility measurements indicate important electronic delocalization that is mainly controlled by composition.
© 1999 Academic Press

INTRODUCTION

In last years, $LaNiO_3$ and derived compounds have generated considerable interest (1–7), and the attention has been especially focused on the metal–insulator (M–I) transitions found in some of these systems (8, 9).

$LaNiO_3$ is well known to be a rhombohedrically distorted perovskite which exhibits a metallic character down to 4.2 K (10). The electrical and magnetic properties displayed by this oxide are governed by strong electronic correlation effects which show a Pauli paramagnetism with Stoner enhancement and metallic behavior with a large resistivity ($\approx 10^{-3}\ \Omega$ cm) at room temperature. In this context, we have been interested in the study of materials in which partial substitution of Ni^{3+} in $LaNiO_3$ (e.g., $LaNi_{1-x}M_xO_3$, M = Co, Fe, Cu, Sb, Te, Re, Mn) has been essayed leading to a partial reduction to Ni^{2+}. In some of the above-mentioned systems, M–I transitions were reported to be temperature, composition, or structure driven, and they could be related to Ni mixed-valences (11–22).

In general, the electrical behavior of these perovskite-type materials can be explained in terms of transitions from localized to collective electrons which are often interpreted on the basis of a conduction model, implying hopping activation of carriers when the M–I transition is crossover.

We have been interested in the $LaNi_{1-x}Ti_xO_3$ ($0.05 \leq x \leq \frac{1}{2}$) mixed oxides and especially in the study of physical properties of these materials in relation to the mixed oxidation state on Ni cations.

This paper reports the synthesis, structural characterization, and electrical and magnetic behavior of the $LaNi_{1-x}Ti_xO_3$ compounds. Formally, for $x = 0$ only Ni^{3+} is present and for $x = \frac{1}{2}$ this element is stabilized as Ni^{2+}.

EXPERIMENTAL

The title oxides were prepared by the "liquid mix" technique (23). The synthesis of $LaNi_{1-x}Ti_xO_3$ ($0.05 \leq x \leq \frac{1}{2}$) materials was carried out in air, starting from $La(NO_3)_3 \cdot 6H_2O$, $Ni(NO_3)_2 \cdot 6H_2O$, and $C_{10}H_{14}O_5Ti$ (supplied by Fluka, Panreac, and Merck, respectively). The temperature employed in the synthesis ranged between 723 and 1073 K for several days, as described elsewhere (16). During the thermal treatment, the samples were reground in each step, and the process was monitored by X-ray diffraction until single and pure phases were obtained. The average formal nickel valence, and hence the total oxygen content, was determined using a standard iodometric technique. Approximately 50 mg sample and an excess of KI were stirred in 25 ml water; concentrated hydrochloric acid was then added dropwise until the dissolution of all solids. Several drops of starch indicator were added to the samples, giving a dark-blue color. The samples were then titrated to a yellow-clear endpoint using a standard thiosulfate solution.

The X-ray diffraction patterns were recorded with a Philips X'Pert-MPD diffractometer with a PW 3050/00 goniometer, using Ni-filtered Cu$K\alpha$ and 2θ step size of 0.05° with a counting time of 12.5 s for each step. The goniometer

0022-4596/99 $30.00
Copyright © 1999 by Academic Press
All rights of reproduction in any form reserved.

was connected to a PC controlled by the commercial program PC-APD (Analytical Powder Diffraction Software, 4.0e).

Electrical conductivity measurements were registered on pelletized samples sintered at 1073 K for 48 h in air, using a d.c. four-probe apparatus according to the Van der Pauw method (24). Colloidal platinum paint was used to make contacts. Thermoelectric power S data were carried out by means of a Keithley 195 A electrometer with an interval impedance of 2×10^7 ohms. To measure e.m.f. (ΔV) a sufficient delay, about 1 h, was allowed after applying the thermal gradient (ΔT) to achieve stability before recording the e.m.f. data.

Magnetic susceptibility data were measured with a SQUID (Quantum Design, MPMS-XL model) with a sensitivity of 10^{-10} emu, in the temperature range 2–300 K in an applied field of 12000 Oe in the phases with $x = 0.10$ and 0.15, and of 1000 Oe in the more substituted phases.

RESULTS AND DISCUSSION

Compositional and Structural Characterization

Table 1 shows the Ni^{3+} concentration and the respective stoichiometry for the $LaNi_{1-x}Ti_xO_3$ series. As can be observed, in general, all the samples analyzed have an oxygen composition very close to the ideal one. The oxygen content was calculated on the basis of the actual amounts of cations in each sample.

The $x = 0$ phase ($LaNiO_3$), was found to have a rhombohedrically distorted perovskite-type structure, S.G. $R\bar{3}c$ (No. 167), whose hexagonal parameters are $a = 5.446(1)$ Å and $c = 13.154(2)$ Å, as was previously reported (17).

The diffraction data for the compounds with a titanium content $x \leq 0.15$ were refined considering a rhombohedral symmetry and the same space group $R\bar{3}c$. This fact indicates that for lower degrees of substitution the parent structure is maintained. On the other hand, the X-ray diffraction patterns for the compound with $x \geq 0.20$ were all indexed in an orthorhombic unit cell. Table 2 compiles the crystal data and the respective cell volumes for these phases. In all cases the cell volume increases when the Ti concentration is increased, as is depicted in Fig. 1 for V^* (obtained from a hypothetical orthorhombic cell, for better comparison) in the $0 \leq x \leq 0.15$ interval and for V in the remaining compositions. This fact is in accordance with the medium size of the cations which are located in the octahedral B sublattice of these pervoskites: Ni^{3+} ions (0.56 Å) are being substituted by Ti^{4+} ions (0.605 Å), and these ones lead to partial reduction from the first ones giving rise to the greater Ni^{2+} ions (0.69 Å). Thus, $LaNi_{1-x}Ti_xO_3$ phases are structurally related to a perovskite-type, although with different symmetry depending on the degree of x substitution. The evolution of the crystal parameters and the adoption of a particular symmetry could be explained taking into account the charge and size of the involved cations, and these features are compiled in the Goldschmidt factor (29), t [$t = d(\text{A–O})/\sqrt{2}\,d(\text{B–O})$], where d(A–O) and d(B–O) are the bond lengths between both cations and oxygen anions. Table 2 also shows the t values for the title materials, obtained from the Shannon ionic radii. As can be observed, the limit value of t which drives the adoption of rhombohedral *vs* orthorhombic symmetry seems to be higher than 0.98

Rietveld's profile analysis method (25) was applied for refinement of all members from X-ray results, and Figs. 2a and 2b give the observed and calculated X-ray diffraction

TABLE 1
Iodometric Results for $LaNi_{1-x}Ti_xO_3$

Compound	Stoichiometry	Ni^{3+} content
0.05	$LaNi_{0.95}Ti_{0.05}O_{2.98}$	0.86
0.10	$LaNi_{0.90}Ti_{0.10}O_{2.98}$	0.75
0.15	$LaNi_{0.85}Ti_{0.15}O_{2.99}$	0.73
0.20	$LaNi_{0.80}Ti_{0.20}O_{2.98}$	0.56
0.25	$LaNi_{0.75}Ti_{0.25}O_{2.98}$	0.455
0.30	$LaNi_{0.70}Ti_{0.30}O_{2.99}$	0.38
0.40	$LaNi_{0.60}Ti_{0.40}O_{2.98}$	0.15

TABLE 2
Cell Parameters and Cell Volumes for $LaNi_{1-x}Ti_xO_3$

x	a (Å)	b (Å)	c (Å)	V (Å^3)	V^* (Å^3)	t	S.G.
0	5.446(1)	5.446(1)	13.154(1)	338.1	225.2	0.996	$R\bar{3}c$
0.05	5.460(1)	5.460(1)	13.176(1)	340.2	226.8	0.991	$R\bar{3}c$
0.10	5.468(1)	5.468(1)	13.215(1)	342.2	228.2	0.987	$R\bar{3}c$
0.15	5.480(1)	5.480(1)	13.252(2)	344.6	229.8	0.983	$R\bar{3}c$
0.20	5.426(1)	5.499(1)	7.762(1)	231.7		0.978	*Pbnm*
0.25	5.448(1)	5.519(1)	7.806(1)	234.7		0.974	*Pbnm*
0.30	5.463(1)	5.530(1)	7.827(1)	236.5		0.970	*Pbnm*
0.40	5.457(1)	5.553(1)	7.867(2)	238.4		0.961	*Pbnm*
0.50	5.517(1)	5.550(1)	7.856(2)	240.6		0.953	*Pbnm*

Note. V^* is volume (in Å^3) corresponding to a hypothetical orthorhombic cell, calculated from $a_0 \approx b_0 \approx a_h$; $c_0 \approx (\sqrt{3}/3)c_h$.

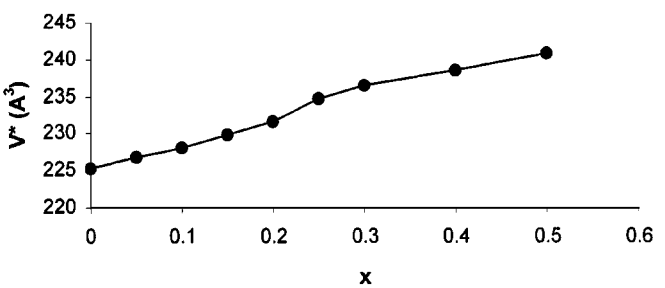

FIG. 1. Variation of V^* vs x for $LaNi_{1-x}Ti_xO_3$.

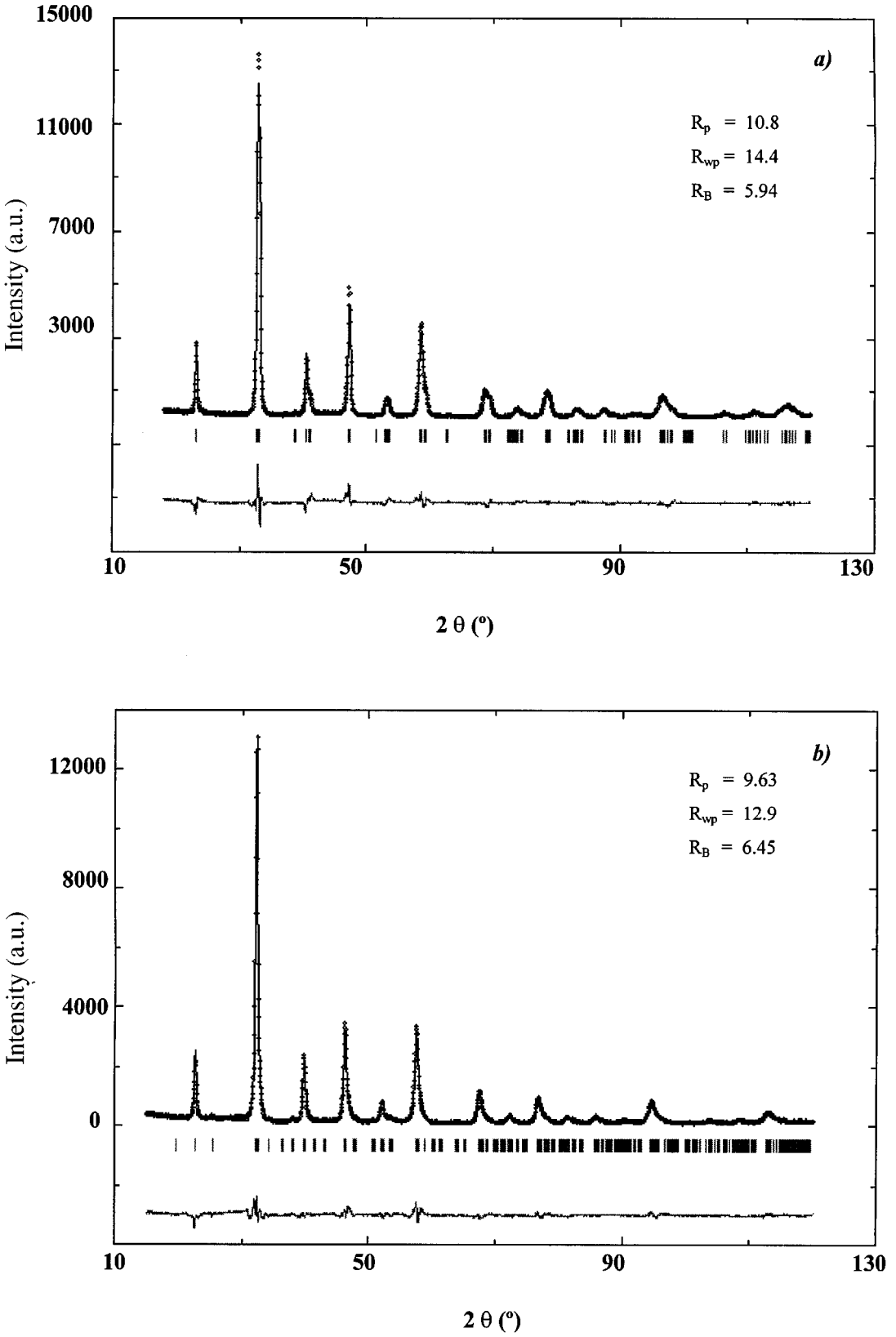

FIG. 2. Observed (dots) and calculated (solid line) X-ray diffraction profiles for (a) the rhombohedral $LaNi_{0.90}Ti_{0.10}O_3$ and (b) the orthorhombic $LaNi_{0.50}Ti_{0.50}O_3$.

TABLE 3
Crystal Data, Atom Coordinates, and Bond Lengths (Å) for $LaNi_{0.90}Ti_{0.10}O_3$

$a = b = 5.468(1)$, $c = 13.215(1)$ (Å), S.G. $R\bar{3}c$				
Atom	Position	x	y	z
La	6*a*	0	0	0.25
Ni/Ti	6*b*	0	0	0
O(1)	18*e*	0.462(2)	0	0.25
La–O	2.94(1)		(Ni/Ti)–O	1.936(1) × 2
	2.52(1)			1.936(9) × 2
	2.941(6) × 2			1.936(7) × 2
	2.527(6) × 2			
	2.717(1) × 2			
	2.717(6) × 2		Mean	1.94
	2.717(5) × 2		Shannon	1.97
Mean	2.73			
Shannon (c.n. = 12)	2.76			

profiles, the difference between them, and the allowed reflections for $x = 0.10$ and $x = 0.50$, respectively. In Table 3 the crystal data, S.G., and the *R*-factors obtained in the refinement for $LaNi_{0.90}Ti_{0.10}O_3$ are gathered, and the profile agreement and the *R*-factors obtained seem to confirm the validity of the proposed structural model. The most representative bond lengths for this sample are given in the same table. In these rhombohedral phases, each Ni/Ti atom is surrounded by six equidistant O atoms, indicating that the distortion within an Ni–O octahedron is very small. There are three types of La–O distances for the rhombohedral $LaNi_{0.90}Ti_{0.10}O_3$, and they are equally separated by 0.20 Å. In the absence of a sharp discontinuity in the increasing La–O distances, it would be proper to assign a coordination number of 12 for the La ion. Comparison between the values and the sums of Shannon ionic radii (26) seems to indicate the reliability of the above assumptions.

It was suggested (27) that the rhombohedral distortion can be viewed as a rotation of the octahedron around the threefold axis by an angle ω from the ideal perovskite position. The angle of rotation ω may be calculated from the oxygen positions using $\omega = \arctan(\sqrt{3} - x\sqrt{12})$; the values of ω calculated for 0.05, 0.10, and 0.15 are 8.03°, 7.48°, and 7.60°, respectively, showing that the octahedral tilt remains relatively large for the rhombohedral phase.

The agreement between the observed and calculated profiles is shown in Fig. 2b for the phase with $x = 0.50$, as an example. These compounds were refined in the space group *Pbnm* (No. 62), in a unit cell of size $\sqrt{2}a_0 \times \sqrt{2}a_0 \times 2a_0$. The refined structural parameters for the phase $LaNi_{0.5}Ti_{0.5}O_3$ are listed in Table 4. In this case, titanium and nickel cations were randomly distributed on the octahedral B sites of the perovskite structure. However, as was suggested by Seinen (28), in the case of an $A_2BB'O_6$ type perovskite an ordering of the B and B′ ions can occur whereby each BO_6 octahedron links six $B'O_6$, and vice versa; this distribution is compatible with a monoclinic symmetry (whose parameters are related to ideal perovskite as follows: $\sqrt{2}a_0 \times \sqrt{2}a_0 \times 2a_0$ and $\beta \approx 90°$). All reflections for $LaNi_{0.5}Ti_{0.5}O_3$ could be satisfactorily indexed in the space group $P2_1/n$. The *R*-factors ($R_p = 9.32$, $R_{wp} = 12.4$, $R_{exp} = 5.12$, and $R_B = 6.59$) are lightly higher than for the orthorhombic cell. For this reason we think that the *Pbnm* space group is more adequate for describing the compound structure. To study the distortion within a Ni–O octahedron, the interatomic distances have been calculated and are also listed in Table 4. There are three different Ni–O distances in the octahedron and, as can be seen, the distortion within an Ni–O octahedron is rather considerable, although the average of the three distances that agree with the Shannon ionic radii seems to indicate the reliability of the above assumptions. The values of the La–O interatomic distances vary over a wide range, indicating that the La–O polyhedron is quite distorted. An inspection of the twelve bond lengths shows a discontinuity in the increasing distances, and a division between the eight first-nearest and the four second-nearest oxygen atoms can be made. This discontinuity suggests that it would be a good approximation to assign coordination number eight to La and its polyhedron can be described as a bicapped trigonal prism. The bond distances agree with the sums of the ionic radii given by Shannon (Table 4). Therefore, the coordination number of La decreases from 12 in the aristotype to eight. The void is reduced in size by tilting of the octahedra. Values of the Ni/Ti–O–Ni/Ti angle can be used to study the octahedral tilt; these values are included in Table 4 and are significantly different from the ideal angle of 180° by ≈15.4°, showing that the octahedral tilt is relatively large.

TABLE 4
Crystal Data, Atom Coordinates, and Bond Lengths (Å) for $LaNi_{0.50}Ti_{0.50}O_3$

$a = 5.517(1)$, $b = 5.551(1)$, $c = 7.856(2)$ (Å), S.G. *Pbnm*					
Atom	Position	x	y	z	
La	4*c*	−0.0048(9)	0.0206(4)	0.25	
Ni/Ti	4*b*	0.5	0	0	
O(1)	8*d*	0.281(5)	0.249(6)	0.036(3)	
O(2)	4*c*	0.02(1)	0.499(3)	0.25	
La–O(1)	2.62(3) × 2		(Ni/Ti)–O(1)	1.85(3) × 2	
	2.56(3) × 2			2.10(3) × 2	
	2.84(3) × 2		(Ni/Ti)–O(2)	1.970(5) × 2	
	3.10(3) × 2				
La–O(2)	2.89(2)				
	2.66(2)		Mean	1.97	
	2.89(7)		Shannon	2.05	
	2.62(7)				
			Ni/Ti–O1–Ni/Ti (4)	161.6°	
Mean	2.66		Ni/Ti–O2–Ni/Ti (2)	170.6°	
Shannon (c.n. = 8)	2.56		⟨Ni/Ti–O–Ni/Ti⟩	164.6°	

Conductivity Measurements

The electronic conductivity variation with temperature for the $LaNi_{1-x}Ti_xO_3$ mixed oxides has been measured in the 300–975 K temperature range. Figure 3 shows the variation of σ vs T. It can be observed that the electronic conductivity depends sensibly on the degree of substitution, x. For the more substituted phases ($x = 0.40$ and 0.50), the conductivity varies exponentially with the temperature (Fig. 3c), whereas in the intermediate ones ($x = 0.25$ and $x = 0.30$) the conductivity is practically temperature-independent (Fig. 3b). And finally, for lower titanium contents ($x \leq 0.20$), a metallic behavior is observed (Fig. 3a), as occurs in the nondoped material, $LaNiO_3$.

Therefore, the $LaNi_{1-x}Ti_xO_3$ systems, shows an interesting metal–insulator (M–I) transition that depends basically on the composition. This behavior seems to be associated with a transition from collective to localized electrons as the x value is increased, 0.25 being the critical value for such transition. Moreover, to analyze the temperature influence on the conductivity, Fig. 4 shows experimental values in the 77–300 K range for $x = 0.10$ and $x = 0.30$ samples. In the $x = 0.10$ sample, a similar behavior to that described above is observed, whereas in the $x = 0.30$ material the M–I transition is noticeable around 140 K.

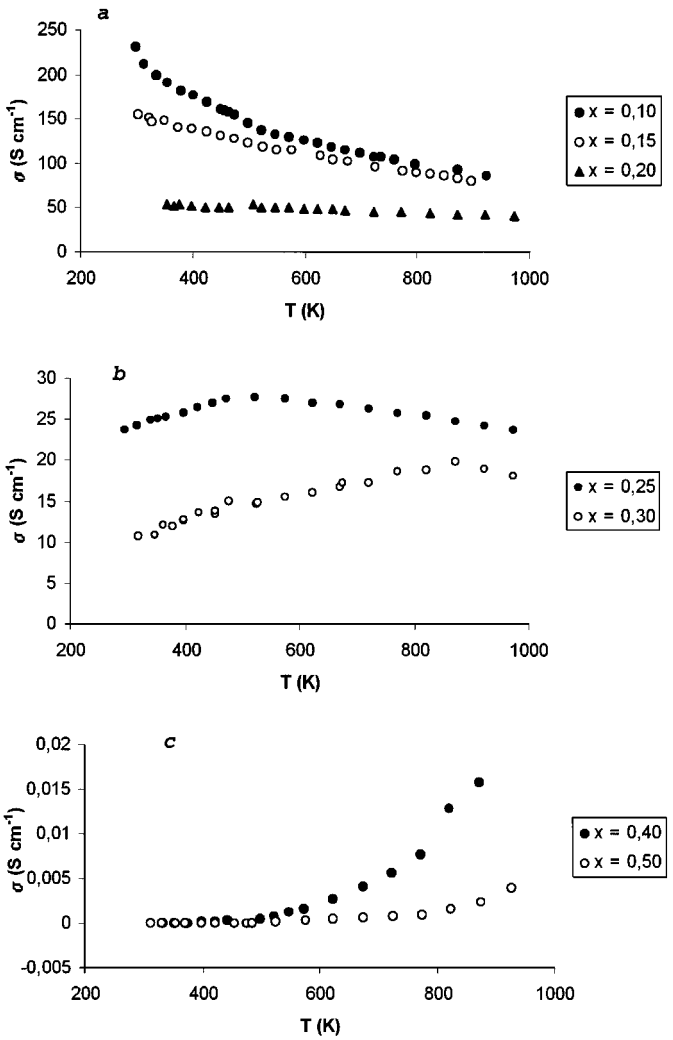

FIG. 3. Variation of σ vs T for $LaNi_{1-x}Ti_xO_3$ in the 300–975 K range.

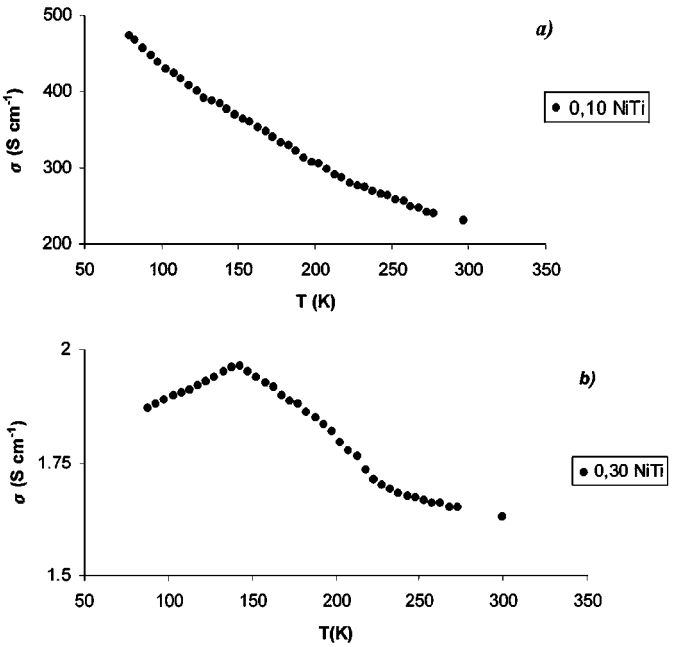

FIG. 4. Variation of σ vs T for (a) $x = 0.10$ and (b) $x = 0.30$ in the 77–300 K range.

In this sense, $LaNiO_3$ ($x = 0$) is well known to behave as a metal down to 0.4 K (10). For the $0.05 \leq x \leq 0.20$ phases, an analogous metallic behavior is observed, although the resistivity values obtained at room temperature are relatively high for a metal ($\rho \approx 10^{-2}\,\Omega$ cm, compared with $\sim 10^{-3}\,\Omega$ cm in pure $LaNiO_3$), and this fact could be interpreted in terms of an important electronic correlation from that temperature.

For the next compositions, $x = 0.25$ and $x = 0.30$, an almost linear dependence between temperature and conductivity is observed and experimental data on conductivity can be fitted to a power-law equation of the type $\sigma(T) = \sigma_0(0) + \sigma_1 T^{\alpha}$ with $\alpha = 0.95$ for both compositions, $\sigma_1 =$ 0.028 and 0.021 (S cm^{-1} K$^{-\alpha}$) for 0.25 and 0.30, respectively. This kind of linear variation of the conductivity with temperature is not very usual in mixed oxides, although it has been previously described in some cases (8). This general behavior takes place in systems that show on M–I transition controlled by the composition, usually for the phase whose composition is close to the transition. On the other hand, the conductivity values obtained for the phases with higher

titanium content ($x > 0.30$) cannot be fitted to a power-law. The dependence between temperature and conductivity for these phases ($0.40 \leq x \leq 0.50$) is characteristic of semiconductor materials; the conductivity data for them were fitted to an exponential law as $\sigma = (A/T) \exp(-E_a/kT)$, which is usually attributed to a small polaron hopping mechanism, where E_a is the activation energy related to the hopping process, A the pre-exponential factor, k the Boltzmann constant, and T the absolute temperature. Figure 5 shows the linear variation of $\ln(\sigma T)$ vs T^{-1} for these phases, which agrees well with the above assumption and supports the validity of a small polaron hopping model for the electronic transport process in these materials, for which the respective activation energy values are of the same order.

The variation of the Seebeck coefficient with temperature has been measured for some of the title compounds between 300 and 923 K, in order to evaluate both the predominant activation process (mobility or carrier concentration) and the sign of the main charge carriers.

Some examples of the variation of the Seebeck coefficient with inverse temperature ($x = 0.10$ and 0.50) are depicted in Fig. 6. For the composition interval $0.05 \leq x \leq 0.30$ negative values of this coefficient have been obtained, suggesting that the conduction process is mainly due to electrons. The absolute values of the Seebeck coefficient slowly increase with temperature for $x = 0.10$. This fact, together with the small values that are measured (lower than 30 μV/K), is characteristic of materials near metallic behavior (30). In contrast, for the composition with $x = 0.50$, positive values were always found in the whole temperature range, which are indicative that holes are the main charge carriers. These results seem to be related to the Ni^{2+}/Ni^{3+} relative amounts in the respective compounds (from $x > 0.30$ there is a clear majority of Ni^{2+}). When Ni^{2+} content predominates in the samples the electrons are more localized on the

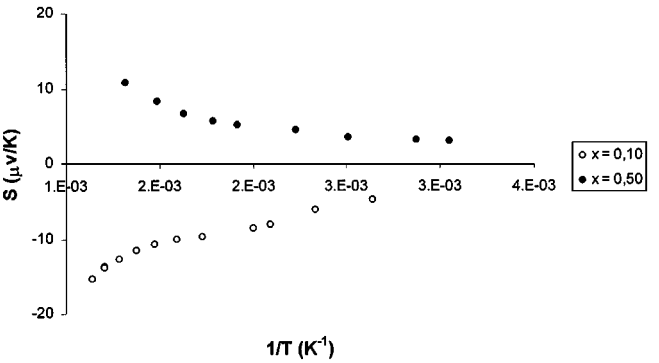

FIG. 6. Variation of the Seebeck coefficient with inverse temperature for $x = 0.10$ and 0.50 in the 323–923 K range.

cations and charge transport is mainly due to polarons which consist of trapped electrons. On the other hand, the nearly temperature independent behavior of the Seebeck coefficient, for the more substituted phases, is in good agreement with a small polarons hopping mechanism mainly driven by mobility activation and with a charge concentration that is almost constant.

The above results allow us to conclude that in the $LaNi_{1-x}Ti_xO_3$ series a composition-driven M–I transition takes place, and it is mainly governed by the relative amounts of Ni^{2+}/Ni^{3+}.

Magnetic Characterization

Figure 7 shows the variation of magnetic susceptibility with temperature (in the 2 and 300 K range) for three compositions that are representative of the general behavior of the system $LaNi_{1-x}Ti_xO_3$. The applied magnetic field was 12000 Oe for $x \leq 0.15$ and 1000 Oe for the more substituted materials, $x \geq 0.20$. A nearly temperature-independent

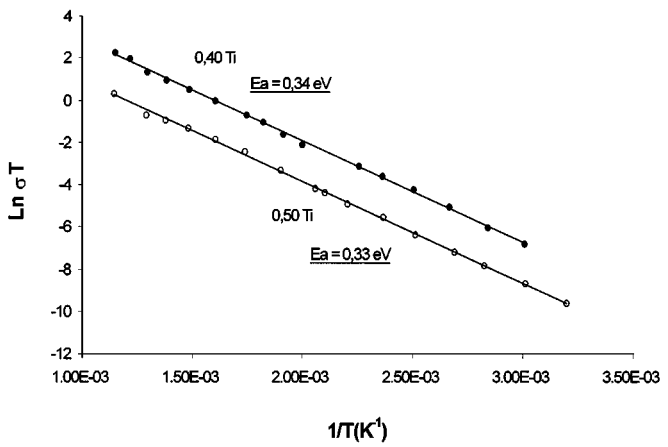

FIG. 5. Variation of $\ln \sigma T$ vs T^{-1} for $x = 0.40$ and $x = 0.50$ in the 300–950 K range.

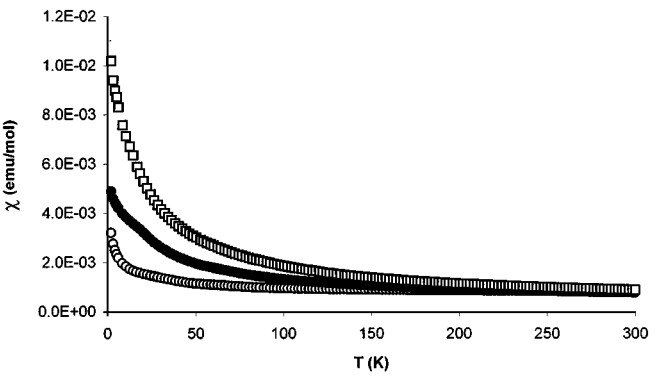

FIG. 7. Variation of the magnetic susceptibility vs temperature for $LaNi_{1-x}Ti_xO_3$ ($x = 0.15$ (○), 0.30 (●), and 0.50 (□)).

TABLE 5
Observed and Calculated Magnetic Moments in the Paramagnetic Part

x	% Ni^{3+}	ΔT (K)[a]	$\mu_{c\,(HS)}$ (MB)[b]	μ_0 (MB)[c]	$\mu_{c\,(LS)}$ (MB)[b]	θ (K)[c]
0.05	90	4.2–50	3.73	0.39	1.76	−13.3
0.10	80	4.2–60	3.58	0.41	1.79	−10.86
0.15	70	4.2–40	3.42	0.42	1.82	−10.22
0.20	60	4.2–40	3.25	0.66	1.84	−29.01
0.25	50	4.2–100	3.08	0.69	1.87	−18.56
0.30	40	4.2–100	2.90	0.70	1.90	−5.01
0.40	20	4.2–100	2.49	0.75	1.95	−1.57
0.50	0	4.2–100	2.00	0.93	2.00	−3.95

[a]Temperature range utilized for the fit.
[b]Magnetic moment calculated from the Curie constant considering high-spin (HS) and low-spin (LS) for the Ni^{3+} ion.
[c]Magnetic moment and Weiss constant obtained from the Curie–Weiss law fit.

variation can be observed above 150 K, and this fact seems to be related to the existence of an important electronic delocalization in the system. Below ~150 K, a marked enhancement of susceptibility values with decreasing temperature is seen, which is more marked as x increases, and this confirms that an electronic localization becomes progressive. Similar results were previously reported for related systems and in the $LaNiO_3$ phase.

The susceptibility data below 100 K were fitted to a Curie–Weiss behavior, and the experimental and calculated (for high-spin and low-spin, of Ni^{3+} ions) magnetic moments are gathered in Table 5 for the title compounds. It is observed that experimental effective moments are notably lower than those expected for the contribution of isolated paramagnetic cations Ni^{2+} or Ni^{3+}, suggesting the metallic character of these systems. The same behavior was reported for the parent compound, $LaNiO_3$, for which the magnetic moment value was 0.17 BM.

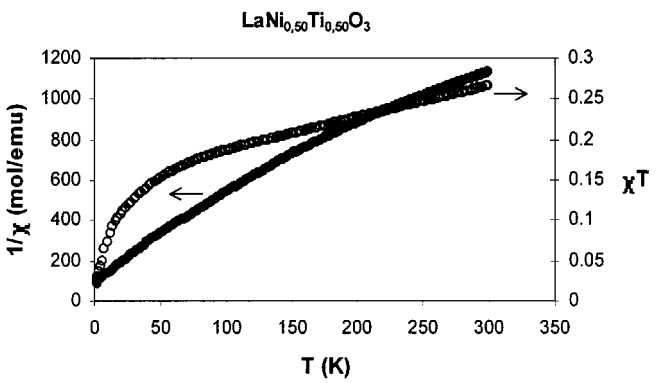

FIG. 8. Variation of the $\chi_m T$ and χ^{-1} for $LaNi_{0.50}Ti_{0.50}O_3$.

The thermal evolution of the $\chi_m T$ and χ^{-1} for $LaNi_{0.5}Ti_{0.5}O_3$ is shown in Fig. 8. The continual decrease observed in the $\chi_m T$ vs T curve is indicative of the presence of an antiferromagnetic ordering, with a Neél temperature value at around 100 K (31).

Therefore, we can conclude that $LaNi_{1-x}Ti_xO_3$ perovskite-type phases show a magnetic behavior in which the electronic localization is controlled by composition, as occurs in related systems.

ACKNOWLEDGMENTS

We are indebted to the CICYT (MAT 97-0326-C04-03) for financial support. We acknowledge the C.A.I. for collecting data on susceptibility and X-ray diffraction.

REFERENCES

1. A. A. Yaremchenko, V. V. Kharton, A. P. Viskup, E. N. Naumovich, N. M. Lapchuk, and V. N. Tikhonovich, *J. Solid State Chem.* **142,** 325 (1999).
2. R. Mahesh, K. R. Kannen, and C. N. R. Rao, *J. Solid State Chem.* **114,** 294 (1995).
3. M. J. Martínez-Lope and J. A. Alonso, *Eur. J. Solid State Inorg. Chem.* **32,** 373 (1995).
4. I. Álvarez, M. L. Veiga, and C. Pico, *J. Solid State Chem.* **136,** 313 (1998).
5. Z. Zhang and M. Greenblatt, *J. Solid State Chem.* **11,** 145 (1994).
6. K. Sreedhar, M. McElfresh, D. Perry, D. Kim, P. Metcalf, and J. M. Honig, *J. Solid State Chem.* **110,** 208 (1994).
7. J. A. Alonso, M. J. Martínez-Lope, and M. Hidalgo, *J. Solid State Chem.* **116,** 146 (1995).
8. A. K. Raychaudhuri, *Phys. Rev. B* **44,** 8572 (1991).
9. M. Imada, *J. Phys. Soc. Jpn.* **62,** 1105 (1993).
10. K. P. Rajeev, G. V. Shivashankar, and A. K. Raychaudhuri, *Solid State Commun.* **79,** 591 (1991).
11. K. Asai, H. Sekizawa, K. Mizashima, and S. Iida, *J. Phys. Soc. Jpn.* **45,** 1417 (1978).
12. K. P. Rajeev and A. K. Raychaudhuri, *Phys. Rev. B* **46,** 1309 (1992).
13. I. Alvarez, M. L. Veiga, and C. Pico, *J. Mater. Chem.* **5,** 1049 (1995).
14. Z. Zhang, M. Greenblatt, and J. B. Goodenough, *J. Solid. State Chem.* **108,** 402 (1994).
15. M. A. Subramanian and G. V. Subba Rao, *J. Solid State Chem.* **31,** 329 (1980).
16. I. Alvarez, J. L. Martínez, M. L. Veiga, and C. Pico, *J. Solid State Chem.* **125,** 47 (1996).
17. C. N. R. Rao, O. M. Parkash, and P. Ganguly, *J. Solid State Chem.* **15,** 186 (1975).
18. N. Y. Vasanthacharya, P. Ganguly, J. B. Goodenough, and C. N. R. Rao, *J. Phys. C Solid State Phys.* **17,** 2745 (1984).
19. N. Y. Vasanthacharya, A. K. Raychaudhuri, P. Ganguly, and C. N. R. Rao, *J. Magn. Mater.* **81,** 133 (1989).
20. K. Motida, *J. Phys. Soc. Jpn.* **43,** 53 (1977).
21. G. V. Bazuev, V. N. Krasilnikov, N. A. Kirsanov, and N. V. Lukin, *Physica C* **230,** 163 (1994).
22. I. Alvarez, M. L. Veiga, and C. Pico, *Solid State Ionics* **91,** 265 (1996).
23. M. Pechini, *U.S.P.* **3,** 231 (1966).
24. L. J. Van der Pauw, *Philips Research Rep.* **1,** 13 (1958).

25. J. Rodríguez-Carvajal, Fullprof: A Program for Reitveld Refinement and Pattern Matching Analysis, Abstracts of Satellite Meeting on Powder Diffraction, XV Congress of International Union of Crystallography, Tolouse, p. 127, 1990. [Revised version, 1994].
26. R. D. Shannon, *Acta Crystallogr*. **32,** 751 (1976).
27. B. G. Hyde and Sten Anderson, "Inorganic Crystal Structures." Wiley–Interscience, New York, 1989.
28. P. A. Seinen, F. P. F. Van Berkel, W. A. Groen, and D. J. W. Ijdo, *Mater. Res. Bull*, **22,** 535 (1987).
29. Goldschimdt, *Metallurgia* **62,** 241 (1960).
30. P. A. Cox, "Transition Metal Oxides. An Introduction to Their Electronic Structure and Properties." Clarendon, Oxford, 1992.
31. I. Gil de Muro, M. Insausti, L. Lezama, J. L. Pizarro, M. I. Arriortua, and T. Rojo, *Eur. J. Inorg. Chem*., 935 (1999).